AIAA JOURNAL
Vol. 30, No. 4, April 1992

Nonlinear Postbuckling Analysis of Plates and Shells by Four-Noded Strain Element

George Z. Voyiadjis* and Guangyu Shi†
Louisiana State University, Baton Rouge, Louisiana 70803

This paper deals with the nonlinear postbuckling analysis of plates and shells by the finite element method. The four-noded C^o strain element for nonlinear plate anaysis developed by the authors is first extended to the nonlinear shell analysis and then used for the nonlinear postbuckling analysis of plates and shallow shells. The element tangent stiffness matrix presented here is given explicitly, i.e., without any numerical integration. Consequently, this C^o strain element is much more computationally economical and efficient than the widely used elements obtained from numerical integration. The efficiency and accuracy of the present four-noded strain element for postbuckling analysis are demonstrated by five numerical examples of various plates and shells.

Nomenclature

A_b, A_m, A_s, A_θ = square matrices used for bending, membrane, transverse shear strain, and slope discretization, respectively
B_b, B_m, B_s, G = strain-displacement matrices for bending, membrane strain, transverse shearing, and slope field, respectively
C_b, C_m, C_s, C_θ = strain-discretization matrices for bending, membrane strain, transverse shearing, and slope field, respectively
D, S, T = bending, stretching, and transverse shearing rigidity matrices, respectively
E = Young's modulus
E = unit base vectors of the fixed global coordinates
e_b, e_m, e_s, θ = increments of bending, in-plane, transverse shear strains, and slopes of an element
${}^k e$ = unit base vectors of the element local coordinates at configuration k
${}^k e_s$ = unit base vectors of the nodal surface coordinates at configuration k
${}^k F$ = in-plane stress resultant matrix at configuration k
f_e, F_{unb} = element internal nodal forces and system unbalanced forces, respectively
K_e, K_b = element tangent stiffness matrices in element local and base coordinates, respectively
$K_g, \Delta q_g$ = global tangent stiffness matrix and global nodal displacement increments of a system
K_L, K_σ = linear and nonlinear parts of K_e, respectively
${}^k M, {}^k N, {}^k Q$ = stress couple, in-plane stress, and transverse shear resultant vectors at configuration k, respectively
${}^k R$ = transformation matrix from E to ${}^k e$
${}^k R_s$ = transformation matrix from E to ${}^k e_s$
${}^k S$ = transformation matrix from ${}^k e$ to ${}^k e_s$
${}^k T_b$ = transformation matrix from Δq_e to Δq_b
P_b, P_m, P_s, P_θ = element strain interpolation matrices for bending, membrane strain, transverse shearing, and slope field, respectively
$T_{\theta i}$ = transformation matrix of large rotations
α_b = element bending strain parameters
$\Delta U_{1i}, \Delta U_{2i}, \Delta U_{3i}$ = nodal displacement increments in global coordinates
$\Delta u_i, \Delta v_i, \Delta w_i$ = nodal displacement increments in element local coordinates
$\Delta q_e, \Delta q_b$ = element nodal displacement increments in element local and base coordinates, respectively
$\Delta\phi_{s1i}, \Delta\phi_{s2i}$ = nodal rotation increments in nodal base coordinates
$\Delta\phi_{xi}, \Delta\phi_{yi}$ = nodal rotation increments in element local coordinates
$\varepsilon_b, \varepsilon_m, \varepsilon_s, \theta$ = element bending, membrane, transverse shear strain, and slope fields, respectively
ν = Poisson's ratio
Ω = element domain

Introduction

THE buckling behavior of plates and shells is quite different from that of columns. For a slender straight column subjected to gradually increasing compressive loads at its ends, the column will become unstable and buckle when the applied loads reach a certain value, i.e., the critical load. The column, in general, will collapse completely when a slight incremental load is applied beyond the critical load. However, the load-carrying capability of plates and shells can be far beyond the critical loads predicted by the stability analysis. This can be demonstrated by the huge discrepancies between results given by the classical stability theory of plates and shells and the experimental observations. Von Karman and Tsien[1] first showed that such buckling behavior of plates and shells is attributed to the highly unstable and nonlinear postbuckling phenomena exhibited by thin structures. Therefore, the nonlinear postbuckling analysis of plates and shells is very useful if one wants to optimize the use of materials in plate and shell structures. Because the rigorous solution of nonlinear postbuckling is impossible in most cases, some approximate numerical methods have to be resorted to in the nonlinear postbuckling analysis.

Received Jan. 21, 1991; revision received April 16, 1991; accepted for publication April 17, 1991.

*Professor, Department of Civil Engineering.
†Research Associate; currently at the Research Institute of Engineering Mechanics, Dalian University of Technology, Dalian, China.

Because of the increased use of shells and plates in the aerospace and nuclear industry, instability analysis of these structures has become more and more important lately. With the advent of the computers and the finite element technique, the engineer's ability to solve complex structural problems has been improved. Numerous finite element models for the large displacement and postbuckling analysis of plates and shells have been suggested (e.g., see Refs. 2–8, among others). However, in most nonlinear finite elements, the element matrices are evaluated through numerical integration. The implementation of numerical integration is very time consuming. Consequently, the elements employing numerical integration are very computationally expensive in nonlinear analysis since the element matrices have to be evaluated numerous times.

A simple four-node, with five degrees of freedom at each node, assumed strain element was developed for plate bending nonlinear analysis by the authors.[9] The element formulation is based on the updated Lagrangian formulation, the von Karman assumption, and the quasiconforming element method (an assumed strain method).[10] Unlike most nonlinear plate elements in which the element matrices are obtained from numerical integration, the element tangent stiffness matrix presented in Ref. 9 is given explicitly. Because of the explicit form of the tangent stiffness matrices, this nonlinear element is extremely economical in the geometrically nonlinear analysis of shear deformable plates. Furthermore, this four-noded quadrilateral element can reduce to the corresponding three-noded triangular element.

The objectives of this study are to extend this assumed strain element to nonlinear shell analysis and then apply it to the nonlinear postbuckling analysis of plates and shells. As pointed out by Bathe and Dvorkin, "the extension of a plate element to a general nonlinear shell element represents a major step."[7] The formulation of an explicit element tangent stiffness matrix of the assumed strain plate element presented by the authors[9,11] is briefly introduced in the next section in which the emphasis is on the evaluation of the initial surface coordinates for large deformation analysis of shells. The postbuckling analysis using this element is performed on a number of structures and compared with the existing analytical/numerical solutions where they are available. These numerical examples demonstrate that the proposed nonlinear plate element, in spite of its simplicity, is not only efficient but also accurate.

Element Tangent Stiffness Matrix

The element considered here is the four-noded quadrilateral strain element, and each node has five degrees of freedom, three translations, and two rotations. The element formulation for the nonlinear analysis of plates was presented in the authors' previous paper.[9] This element is extended to the nonlinear shell analysis in the present study. Some basic equations will be presented here again for self-completeness.

Element Tangent Stiffness Matrix in the Element Local Coordinates

The von Karman assumptions and the updated Lagrangian formulation are used here to derive the element tangent stiffness matrix. In the finite element modeling of transverse shear deformable plates using the generalized displacement method, the incremental bending strains $\boldsymbol{\varepsilon}_b$, membrane strains $\boldsymbol{\varepsilon}_m$, transverse shear strains $\boldsymbol{\varepsilon}_s$, and slopes $\boldsymbol{\theta}$ of an element defined in the element local coordinates take the forms

$$\boldsymbol{\varepsilon}_b = \begin{Bmatrix} \dfrac{\partial \Delta\phi_x}{\partial x} \\ \dfrac{\partial \Delta\phi_y}{\partial y} \\ \dfrac{\partial \Delta\phi_x}{\partial y} + \dfrac{\partial \Delta\phi_y}{\partial x} \end{Bmatrix} \approx \boldsymbol{B}_b \Delta \boldsymbol{q}_e \tag{1}$$

$$\boldsymbol{\varepsilon}_m = \begin{Bmatrix} \dfrac{\partial \Delta u}{\partial x} \\ \dfrac{\partial \Delta v}{\partial y} \\ \dfrac{\partial \Delta u}{\partial y} + \dfrac{\partial \Delta v}{\partial x} \end{Bmatrix} \approx \boldsymbol{B}_m \Delta \boldsymbol{q}_e \tag{2}$$

$$\boldsymbol{\varepsilon}_s = \begin{Bmatrix} \dfrac{\partial \Delta w}{\partial x} - \Delta\phi_x \\ \dfrac{\partial \Delta w}{\partial y} - \Delta\phi_y \end{Bmatrix} \approx \boldsymbol{B}_s \Delta \boldsymbol{q}_e \tag{3}$$

$$\boldsymbol{\theta} = \begin{Bmatrix} \dfrac{\partial \Delta w}{\partial x} \\ \dfrac{\partial \Delta w}{\partial y} \end{Bmatrix} \approx \boldsymbol{G} \Delta \boldsymbol{q}_e \tag{4}$$

where Δw denotes the increment of the generalized transverse displacement across the plate thickness; $\Delta\phi_x$ and $\Delta\phi_y$ represent the increments of generalized rotations of cross sections of the plate. By using the principle of virtual work, the element tangent stiffness matrix in the element local coordinates (x, y) at configuration k, $\boldsymbol{K}_e$ takes the form[6,9]

$$\boldsymbol{K}_e = \boldsymbol{K}_L + \boldsymbol{K}_\sigma \tag{5}$$

with

$$\boldsymbol{K}_L = \int_\Omega (\boldsymbol{B}_b^T \boldsymbol{D} \boldsymbol{B}_b + \boldsymbol{B}_m^T \boldsymbol{S} \boldsymbol{B}_m + \boldsymbol{B}_s^T \boldsymbol{T} \boldsymbol{B}_s)\, dx\, dy \tag{6}$$

$$\boldsymbol{K}_\sigma = \int_\Omega \boldsymbol{G}\, {}^k\boldsymbol{F} \boldsymbol{G}\, dx\, dy \tag{7}$$

$${}^k\boldsymbol{F} = \begin{bmatrix} {}^kN_x & {}^kN_{xy} \\ {}^kN_{xy} & {}^kN_y \end{bmatrix} \tag{8}$$

The left superscript k always represents configuration k and the right superscript T denotes the transpose of matrix in this study. As shown in Eq. (7), $\boldsymbol{K}_\sigma$ is associated with the in-plane stress resultants. $\boldsymbol{K}_\sigma$ takes into account the geometric nonlinearity including the postbuckling behavior of a structure.

In the authors' previous work,[9] the element strain-displacement matrices $\boldsymbol{B}_b$, $\boldsymbol{B}_m$, and $\boldsymbol{B}_s$ as well as the slope-displacement matrix $\boldsymbol{G}$ are evaluated by the quasiconforming element method.[10] The starting point in the formulation of a quasiconforming element is to interpolate element strain fields in terms of the undetermined strain parameters, which are the element local quantities. For example, the bending strains $\boldsymbol{\varepsilon}_b$ defined in Eq. (1) can be approximated as

$$\boldsymbol{\varepsilon}_b \approx \boldsymbol{P}_b \boldsymbol{\alpha}_b \tag{9}$$

If one lets $\boldsymbol{W}_b$ be the test functions, then the weak form of Eqs. (1) and (9) may be written as

$$\int_\Omega \boldsymbol{W}_b (\boldsymbol{\varepsilon}_b - \boldsymbol{P}_b \boldsymbol{\alpha}_b)\, d\Omega = 0 \tag{10}$$

in which Ω signifies the domain of the element under consideration. In order to have a symmetric stiffness matrix, the test functions can be taken as $\boldsymbol{W}_b = \boldsymbol{P}_b^T$. By carrying out the integration, this equation leads to

$$\boldsymbol{A}_b \boldsymbol{\alpha}_b = \boldsymbol{C}_b \Delta \boldsymbol{q}_e \quad \text{or} \quad \boldsymbol{\alpha}_b = \boldsymbol{A}_b^{-1} \boldsymbol{C}_b \Delta \boldsymbol{q}_e \tag{11}$$

with

$$\boldsymbol{A}_b = \int_\Omega \boldsymbol{P}_b^T \boldsymbol{P}_b \, d\Omega, \qquad \boldsymbol{C}_b \Delta \boldsymbol{q}_e = \int_\Omega \boldsymbol{P}_b^T \boldsymbol{\varepsilon}_b \, d\Omega \tag{12}$$

where $\boldsymbol{A}_b$ is a symmetric and nonsingular matrix. Substituting for $\boldsymbol{\alpha}_b$ in Eq. (9) from Eqs. (11), then Eqs. (1) and (9) give

$$\boldsymbol{B}_b = \boldsymbol{P}_b \boldsymbol{A}_b^{-1} \boldsymbol{C}_b \tag{13}$$

Similarly, one has

$$\boldsymbol{B}_m = \boldsymbol{P}_m \boldsymbol{A}_m^{-1} \boldsymbol{C}_m \tag{14}$$

$$\boldsymbol{B}_s = \boldsymbol{P}_s \boldsymbol{A}_s^{-1} \boldsymbol{C}_s \tag{15}$$

$$\boldsymbol{G} = \boldsymbol{P}_\theta \boldsymbol{A}_\theta^{-1} \boldsymbol{C}_\theta \tag{16}$$

Equations (9–16) indicate that the element strain fields in quasiconforming elements are obtained from integration instead of differentiation used in the conventional assumed displacement elements. For the four-noded quadrilateral element considered here, the following strain interpolation matrices are employed,

$$\boldsymbol{P}_b = \begin{bmatrix} 1 & x & y & xy & 0 & 0 & 0 & 0 \\ 0 & 0 & 0 & 0 & 1 & x & y & xy \\ 0 & 0 & 0 & 0 & 0 & 0 & 1 & x \; y \end{bmatrix} \tag{17}$$

$$\boldsymbol{P}_m = \begin{bmatrix} 1 & y & 0 & 0 & 0 \\ 0 & 0 & 1 & x & 0 \\ 0 & 0 & 0 & 0 & 1 \end{bmatrix} \tag{18}$$

$$\boldsymbol{P}_s = \begin{bmatrix} 1 & 0 \\ 0 & 1 \end{bmatrix} \tag{19}$$

$$\boldsymbol{P}_\theta = \begin{bmatrix} 1 & x & y & xy & 0 & 0 & 0 & 0 \\ 0 & 0 & 0 & 0 & 1 & x & y & xy \end{bmatrix} \tag{20}$$

where $\boldsymbol{A}_b$, $\boldsymbol{C}_b$, $\boldsymbol{A}_m$, $\boldsymbol{C}_m$, $\boldsymbol{A}_s$, and $\boldsymbol{C}_s$ can be found in the authors' earlier paper,[11] and $\boldsymbol{A}_\theta$ and $\boldsymbol{C}_\theta$ were presented in Ref. 9. All of these matrices are given explicitly.

Substituting Eqs. (13–16) into Eqs. (6) and (7) gives

$$\begin{aligned} \boldsymbol{K}_L = {} & \boldsymbol{C}_b^T \boldsymbol{A}_b^{-1} \int_\Omega \boldsymbol{P}_b^T \boldsymbol{D} \boldsymbol{P}_b \, dx \, dy \, \boldsymbol{A}_b^{-1} \boldsymbol{C}_b \\ & + \boldsymbol{C}_m^T \boldsymbol{A}_m^{-1} \int_\Omega \boldsymbol{P}_m^T \boldsymbol{S} \boldsymbol{P}_m \, dx \, dy \, \boldsymbol{A}_m^{-1} \boldsymbol{C}_m \\ & + \boldsymbol{C}_s^T \boldsymbol{A}_s^{-1} \int_\Omega \boldsymbol{P}_s^T \boldsymbol{T} \boldsymbol{P}_s \, dx \, dy \, \boldsymbol{A}_s^{-1} \boldsymbol{C}_s \end{aligned} \tag{21}$$

$$\boldsymbol{K}_\sigma = \boldsymbol{C}_\theta^T \boldsymbol{A}_\theta^{-1} \int_\Omega \boldsymbol{P}_\theta^T \, {}^k\boldsymbol{F} \boldsymbol{P}_\theta \, dx \, dy \, \boldsymbol{A}_\theta^{-1} \boldsymbol{C}_\theta \tag{22}$$

where the symmetry of $\boldsymbol{A}_b$, $\boldsymbol{A}_m$, $\boldsymbol{A}_s$, and $\boldsymbol{A}_\theta$ is used. The integrals in Eqs. (21) and (22) can be carried out explicitly since the integrands are merely simple polynomials. Consequently, the element tangent stiffness matrix can be obtained explicitly, i.e., without any numerical integration. Compared with the nonlinear elements obtained through numerical integration, the explicit form of the element tangent stiffness matrix presented here makes the resulting element very computationally economical.

The element nodal force vector evaluated in the element local coordinates at configuration k is given by

$$\boldsymbol{f}_e = \int_\Omega (\boldsymbol{B}_b^T \, {}^k\boldsymbol{M} + \boldsymbol{B}_m^T \, {}^k\boldsymbol{N} + \boldsymbol{B}_s^T \, {}^k\boldsymbol{Q}) \, dx \, dy \tag{23}$$

in which $\boldsymbol{B}_b$, $\boldsymbol{B}_m$, and $\boldsymbol{B}_s$ are defined in Eqs. (13–15), respectively; ${}^k\boldsymbol{M}$, ${}^k\boldsymbol{N}$, and ${}^k\boldsymbol{Q}$ take the form

$${}^k\boldsymbol{M} = \begin{Bmatrix} {}^k\boldsymbol{M}_x \\ {}^k\boldsymbol{M}_y \\ {}^k\boldsymbol{M}_{xy} \end{Bmatrix}, \quad {}^k\boldsymbol{N} = \begin{Bmatrix} {}^k\boldsymbol{N}_x \\ {}^k\boldsymbol{N}_y \\ {}^k\boldsymbol{N}_{xy} \end{Bmatrix}, \quad {}^k\boldsymbol{Q} = \begin{Bmatrix} {}^k\boldsymbol{Q}_x \\ {}^k\boldsymbol{Q}_y \end{Bmatrix} \tag{24}$$

Corresponding to the strain interpolation functions given in Eqs. (17–19), a bilinear field for ${}^k\boldsymbol{M}$ and ${}^k\boldsymbol{N}$ and a constant function for ${}^k\boldsymbol{Q}$ are employed here. Similar to Eqs. (21) and (22), the integrals in Eq. (23) can also be carried out explicitly.

Initial Surface Coordinates for Large Deformation Analysis of Shells

A surface coordinate system associated with each nodal point[6] is adopted in the authors' previous work in order to efficiently define the global rotational degrees of freedom. After deformation, say from configuration $k-1$ to k, there will be three rotational components $(\theta_1, \theta_2, \theta_3)$ at a nodal point, and the nodal surface coordinates at node i will undergo a finite rigid-body rotation with components $(\theta_1, \theta_2, \theta_3)_i$. In the authors' previous work, the initial surface coordinates for a flat plate takes the form of a 3×3 identity matrix. The initial surface coordinates for shells will be presented here.

If one lets $\boldsymbol{E}$ be the unit base vectors of the fixed global coordinates and ${}^k\boldsymbol{e}$ and ${}^k\boldsymbol{e}_s$ the unit base vectors of the element local coordinates and the nodal surface coordinates at configuration k, respectively, then the relations between ${}^k\boldsymbol{e}$ and $\boldsymbol{E}$ as well as between ${}^k\boldsymbol{e}_s$ and $\boldsymbol{E}$ take the form

$${}^k\boldsymbol{e} = {}^k\boldsymbol{R} \boldsymbol{E} \tag{25}$$

$${}^k\boldsymbol{e}_s = {}^k\boldsymbol{R}_s \boldsymbol{E} \tag{26}$$

${}^k\boldsymbol{R}$ can be determined easily by the nodal coordinates of the element under consideration. The determination of ${}^k\boldsymbol{R}_s$ will be presented below. It should be noted that ${}^k\boldsymbol{e}$ is associated with a finite element and updates with the changes of the element nodal coordinates, whereas ${}^k\boldsymbol{e}_s$ is related to a nodal point and rotates rigidly with the deformations of the nodal point. The transformation from ${}^{k-1}\boldsymbol{e}_s$ to ${}^k\boldsymbol{e}_s$ at node i can be written as

$${}^k\boldsymbol{e}_{si} = \boldsymbol{T}_{\theta i} \, {}^{k-1}\boldsymbol{e}_{si} = \boldsymbol{T}_{\theta i} \, {}^{k-1}\boldsymbol{R}_{si} \boldsymbol{E} = {}^k\boldsymbol{R}_{si} \boldsymbol{E} \tag{27}$$

in which $\boldsymbol{T}_{\theta i}$ is the transformation matrix of large rotations at node i and is of the form[12]

$$\boldsymbol{T}_{\theta i} = \exp(\hat{\boldsymbol{\Theta}}_i) \tag{28}$$

with

$$\hat{\boldsymbol{\Theta}}_i = \hat{\Theta}_{mn} = \varepsilon_{mnk} \theta_k \qquad (m, n, k = 1, 2, 3) \quad \text{at node } i \tag{29}$$

where ε_{mnk} is the permutation tensor. For the initial surface coordinates ${}^o\boldsymbol{e}_s = \{{}^o\boldsymbol{e}_{s1}, {}^o\boldsymbol{e}_{s2}, {}^o\boldsymbol{e}_{s3}\}$ at a nodal point of a shell, ${}^o\boldsymbol{e}_{s3}$ is chosen to coincide with the outward normal of the undeformed shell surface at the point, and ${}^o\boldsymbol{e}_{s1}$ and ${}^o\boldsymbol{e}_{s2}$ are defined as

$${}^o\boldsymbol{e}_{s1} = \frac{\boldsymbol{E}_2 \times {}^o\boldsymbol{e}_{s3}}{|\boldsymbol{E}_2 \times {}^o\boldsymbol{e}_{s3}|} \tag{30}$$

$${}^o\boldsymbol{e}_{s2} = {}^o\boldsymbol{e}_{s3} \times {}^o\boldsymbol{e}_{s1} \tag{31}$$

where $\boldsymbol{E}_2$ is the second component of the unit base vectors $\boldsymbol{E}$ of the fixed global coordinates, and the symbol $\times$ denotes the cross product. Equations (27) and (25) yield the trans-

formation between ${}^k\boldsymbol{e}_s$ and ${}^k\boldsymbol{e}$ at node i of an element as

$$ {}^k\boldsymbol{e}_{si} = {}^k\boldsymbol{R}_s\, {}^k\boldsymbol{R}^T\, {}^k\boldsymbol{e} = {}^k\boldsymbol{S}\, {}^k\boldsymbol{e} \tag{32} $$

with

$$ {}^k\boldsymbol{S} = {}^k\boldsymbol{R}_s\, {}^k\boldsymbol{R}^T \tag{33} $$

It may be noted that ${}^k\boldsymbol{S}$ is not only associated with a nodal point but also dependent on the element under consideration.

Transformation of Element Stiffness Matrix

In the present study, each node has five degrees of freedom, i.e., three translations and two rotations. At node i of an element, the degrees of freedom defined in the element local coordinates are the incremental translations Δu_i, Δv_i, as well as Δw_i in the directions of ${}^k\boldsymbol{e}_1$, ${}^k\boldsymbol{e}_2$, and ${}^k\boldsymbol{e}_3$ under consideration and two incremental rotations $\Delta\phi_{xi}$ and $\Delta\phi_{yi}$ about $-{}^k\boldsymbol{e}_2$ and ${}^k\boldsymbol{e}_1$. The global degrees of freedom at the same node are the incremental translations ΔU_{1i}, ΔU_{2i}, and ΔU_{3i} measured in the directions of the fixed global coordinates $\boldsymbol{E}_j$ ($j = 1, 2, 3$) as well as rotations $\Delta\phi_{s1i}$ and $\Delta\phi_{s2i}$ about $-{}^k\boldsymbol{e}_{s2}$ and ${}^k\boldsymbol{e}_{s1}$ of the surface coordinate system ${}^k\boldsymbol{e}_s$ at the nodal point. This special combination of the element local coordinates with the nodal surface coordinates is called the base coordinates.[6] The transformation of the incremental displacement parameters at node i from an element local coordinates $\Delta\boldsymbol{q}_{ei}$ to the corresponding base coordinates $\Delta\boldsymbol{q}_{bi}$ takes the form

$$ \Delta\boldsymbol{q}_{bi} = \begin{Bmatrix} \Delta U_{1i} \\ \Delta U_{2i} \\ \Delta U_{3i} \\ \Delta\phi_{s1i} \\ \Delta\phi_{s2i} \end{Bmatrix} = \begin{bmatrix} {}^k\boldsymbol{R}^T & \boldsymbol{0} \\ \boldsymbol{0} & {}^k\boldsymbol{s}_i^* \end{bmatrix} \begin{Bmatrix} \Delta u_i \\ \Delta v_i \\ \Delta w_i \\ \Delta\phi_{xi} \\ \Delta\phi_{yi} \end{Bmatrix} = {}^k\boldsymbol{T}_{bi}\Delta\boldsymbol{q}_{ei} \tag{34} $$

in which ${}^k\boldsymbol{s}_i^*$ is the upper left 2×2 submatrix of matrix ${}^k\boldsymbol{S}$ at node i as defined in Eq. (33) but with a different sequence. Consequently, the global displacement vector $\Delta\boldsymbol{q}_b$ and the local displacement vector $\Delta\boldsymbol{q}_e$ for an element have the following relationship

$$ \Delta\boldsymbol{q}_b = {}^k\boldsymbol{T}_b\Delta\boldsymbol{q}_e \tag{35} $$

For the four-noded element considered here, ${}^k\boldsymbol{T}_b$ is of the form

$$ {}^k\boldsymbol{T}_b = \begin{Bmatrix} {}^k\boldsymbol{T}_{b1} & & \boldsymbol{0} & \\ & {}^k\boldsymbol{T}_{b2} & & \\ & & {}^k\boldsymbol{T}_{b3} & \\ \boldsymbol{0} & & & {}^k\boldsymbol{T}_{b4} \end{Bmatrix} \tag{36} $$

By using Eq. (35), the element tangent stiffness matrix evaluated in the element coordinates $\boldsymbol{K}_e$ given by Eqs. (5–7) can be transformed into the one corresponding to the base coordinates $\boldsymbol{K}_b$ as

$$ \boldsymbol{K}_b = {}^k\boldsymbol{T}_b\boldsymbol{K}_e\, {}^k\boldsymbol{T}_b^T \tag{37} $$

Similarly, the element internal nodal force vector $\boldsymbol{f}_b$ in the base coordinates is given by

$$ \boldsymbol{f}_b = {}^k\boldsymbol{T}_b\boldsymbol{f}_e \tag{38} $$

Solution Algorithm

System Equations

Following the common assembling procedure, one obtains the nodal equilibrium equations of a system for configuration $k + 1$ as

$$ \boldsymbol{K}_g\Delta\boldsymbol{q}_g = \Delta\boldsymbol{P} + \boldsymbol{F}_{\text{unb}} \tag{39} $$

with

$$ \boldsymbol{K}_g\Delta\boldsymbol{q}_g = \sum_{\text{elem}} \boldsymbol{K}_b\Delta\boldsymbol{q}_b \tag{40} $$

$$ \boldsymbol{F}_{\text{unb}} = {}^k\boldsymbol{P} - \sum_{\text{elem}} \boldsymbol{f}_b \tag{41} $$

where $\boldsymbol{K}_g$, $\Delta\boldsymbol{q}_g$, and $\boldsymbol{F}_{\text{unb}}$ are, respectively, the assembled global stiffness matrix, the nodal displacement increment vector, and the unbalanced force vector of the system; $\Delta\boldsymbol{P}$ is the load increment vector from configurations k to $k + 1$; and ${}^k\boldsymbol{P}$ is the total load vector up to configuration k. The unbalanced forces $\boldsymbol{F}_{\text{unb}}$ given in Eq. (41) result from the geometric nonlinearity of the system.

Solution Algorithm

The Newton-Raphson method is adopted in this work to solve the incremental system equations given in Eq. (39) in which the unbalanced forces are resolved by the iteration. The load increments $\Delta\boldsymbol{P}$ are determined by the arc length method.[13–15] It was shown (see Refs. 16, 17, and others) that the arc length method is really a very suitable and efficient approach to deal with snap through and other postbuckling problems. The convergence criterion used here is of the form

$$ \frac{|\Delta\boldsymbol{q}_{g'}|}{|\Delta\boldsymbol{q}_g|} \le e_{\text{tol}} \tag{42} $$

in which $|\Delta\boldsymbol{q}_{g'}|$ denotes the norm of the displacement increments obtained in the latest iteration, $|\Delta\boldsymbol{q}_g|$ represents the norm of the total displacement increments obtained during the current increment, and e_{tol} is a prescribed value of error tolerance. The value of $e_{\text{tol}} = 0.0001$ is used here.

Numerical Examples

The postbuckling analysis of a number of structures is presented in this section. All of the shapes of the elements used in this section, e.g., rectangular, quadrilateral, and triangular, are the variations of the four-noded quadrilateral strain ele-

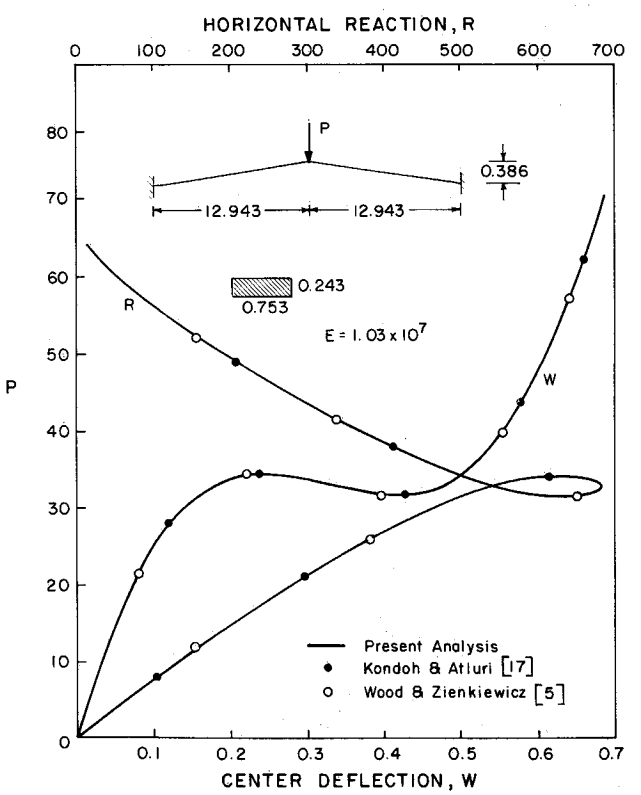

Fig. 1 Load-deflection and load-reaction curves of Williams' toggle.

ment developed by the authors.[9] The numerical solutions obtained by the present element are compared with the existing analytical/numerical solutions where they are available.

Example 1: Williams' Toggle Frame

Williams' toggle is schematically shown in Fig. 1, together with the material properties and the load condition (the units used there are in./lb in order to compare the present results with others directly). The toggle under the central load exhibits snap-through behavior. Four rectangular elements are used for the discretization of a half-span of the toggle. The curves of the central deflection and horizontal reaction at the fixed end vs the applied load are depicted in Fig. 1. The numerical solutions given by Wood and Zienkiewicz[5] as well as Kondoh and Atluri[17] are also plotted here for comparison. It may be noted that present results agree well with the referenced solutions.

Example 2: Simply Supported Circular Plate Subjected to Edge Pressure

A thin, simply supported circular plate subjected to a uniform comprehensive normal stress along the edge is concerned in this example. The geometry and material properties of the circular plate are given in Fig. 2. The critical edge pressure is $q_{crit} = 4.24\ D/R^2h$,[18] where D, R, and h are the bending rigidity, radius, and thickness of the circular plate, respectively. However, the load-carrying capability of this plate is far beyond the critical load. The buckling pattern of the circular plate is symmetric about the plate center.[18] Therefore, only one-quarter of the plate is considered here. Twelve quadrilateral elements are used, as illustrated in Fig. 2. A lateral disturbance force $P = 2\pi Rhq/1000$ is introduced. The deflection at the center and the slope at the edge against the load parameter $\Lambda = q/q_{crit}$ beyond the critical load are plotted in Fig. 2. The parameter γ used in the load-deflection curve is defined as $\gamma = 1\sqrt{12(1-\nu^2)}$. It can be observed that the present numerical results have a good agreement with the analytical solutions given by Friedrichs and Stoker.[18] The slight difference for the load-slope curve when Λ is close to 1 results from the fact that a lateral disturbance load is used in the present numerical analysis.

Example 3: Rectangular Plate Subjected to In-Plane Load

This example concerns the postbuckling analysis of a simply supported rectangular plate subjected to a uniaxial compression along the shorter edges. The in-plane displacements of the simply supported plate are constrained in such a way that the longitudinal edges can move freely in the tangential direction, but are completely restrained in the normal direction. The geometric and material data of the plate are shown in Fig. 3. These data are the same as those used by Allman.[19] In Allman's paper, each transverse end of the plate is assumed to be compressed by a force applied through a rigid end block. Under the given boundary and loading conditions, this rectangular plate will have a symmetric buckling mode.[19] Consequently, only one-quarter of the plate needs to be analyzed.

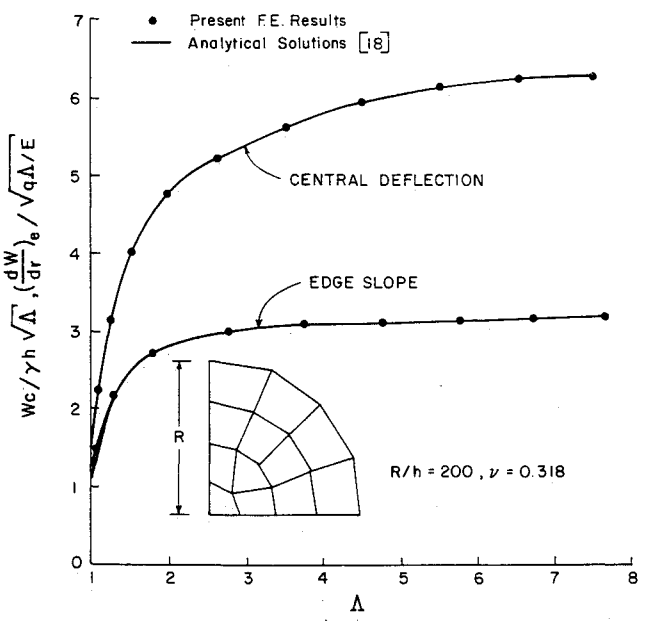

Fig. 2 Central deflection and edge slope curves beyond the critical load for a simply supported circular plate subjected to edge compression.

The rectangular plate undergoes single buckle in the transverse direction. However, it can have a higher buckling mode in the longitudinal direction when the load is large enough. To account for the higher buckling mode more accurately, 2 × 3 and 2 × 6 meshes are considered. The 2 × 3 mesh is illustrated in Fig. 3. The computational model is also depicted in Fig. 3 together with a small lateral disturbance force applied at the plate center. The present results for the average displacement U in the longitudinal direction vs the in-plane load P is graphically shown in Fig. 3 where U and P are defined, respectively, as

$$U = \frac{1}{b}\int_0^b u\left(\frac{-a}{2}, y\right) dy \tag{43a}$$

$$P = bq \tag{43b}$$

The deflections along the central longitudinal line of the plate corresponding to various load values obtained by a 2 × 6 mesh are illustrated in Fig. 4. Figure 4 shows that the plate undergoes buckling from one buckle to three buckles when the load reaches certain a value. Figure 3 indicates that the plate can be in equilibrium in more than one buckle pattern in certain load regions. Figures 3 and 4 also show that the stiffness of the plate becomes negative when the central deflection crosses its initial equilibrium configuration after the large deflection. Allman's results[19] also showed that the plate can be in equilibrium in more than one buckling mode. However, the local drops vertically at the limit point of the U-P curve there. Such vertical drop makes the slop of the curve become infinite at the corresponding point.

Example 4: Hinged Cylindrical Shell Under a Central Load

The geometry and material properties of the circular cylindrical shell under consideration are shown in Fig. 5. The shell is subjected to a concentrated central load on the convex side, as depicted in Fig. 5. The longitudinal edges of the shell are hinged and immovable, whereas the curved edges are completely free. Only one-quarter of the shell is analyzed here because of the symmetry, and a 4 × 4 mesh is used for it. Both triangular and quadrilateral elements are used in this example. The present results of the central deflection vs the

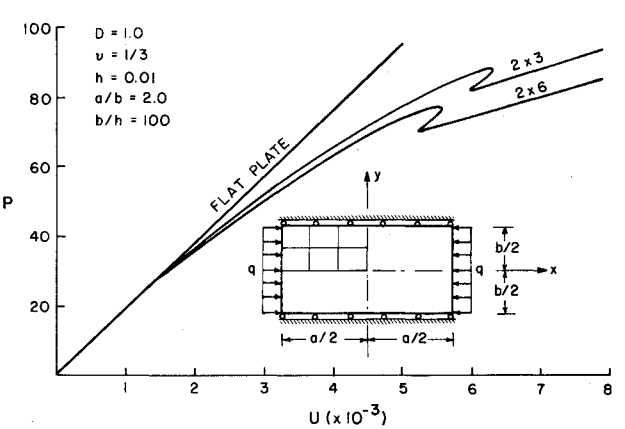

Fig. 3 Rectangular plate under in-plane pressure.

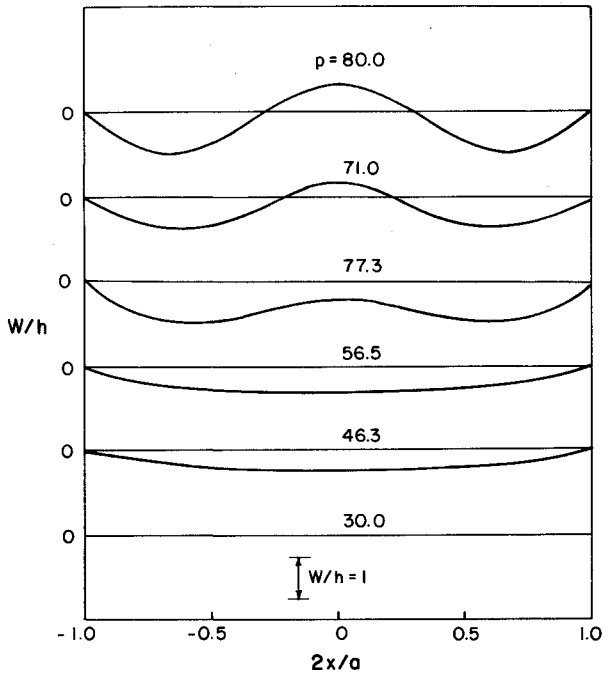

Fig. 4 Deflections along central longitudinal line of rectangular plate under in-plane pressure.

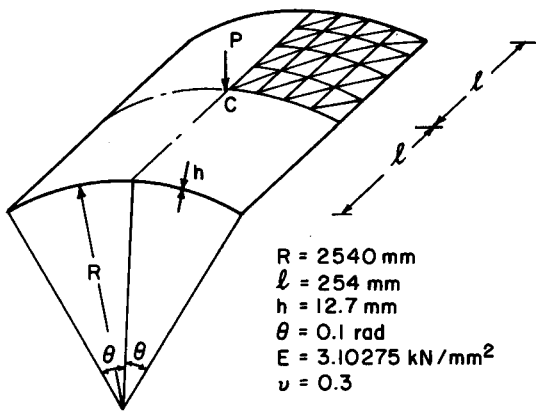

Fig. 5 Geometry, material properties, and element layout of hinged cylindrical shell.

applied central load are plotted in Fig. 6, and the numerical solution obtained by Horrigmore and Bergan[6] are also shown for comparison. The present result obtained from the flat three-noded triangular elements agrees very well with the solution given by Horrigmore and Bergan,[6] whereas the result given by the flat rectangular elements is little bit stiffer. The different performances of the present triangular and rectangular elements can be attributed to the fact that the three-noded triangular elements are able to represent the deformed geometry of the shell more accurately than the four-noded quadrilateral elements do.

Yang and Saigal[20] solved the same problem using a higher order curved shell element (48 degrees of freedom) and a 2 × 2 mesh for a quarter of the shell. Even though less elements are used in Yang and Saigal's solution, more nodal degrees of freedom are used there compared with the finite elements used here. The simple flat-plate elements used in Ref. 6 and in the present study give the results with the same accuracy as the Yang and Saigal's higher order curved element. This indicates that the lower order plate elements are really quite competitive with the higher order shell elements in nonlinear shell analysis.

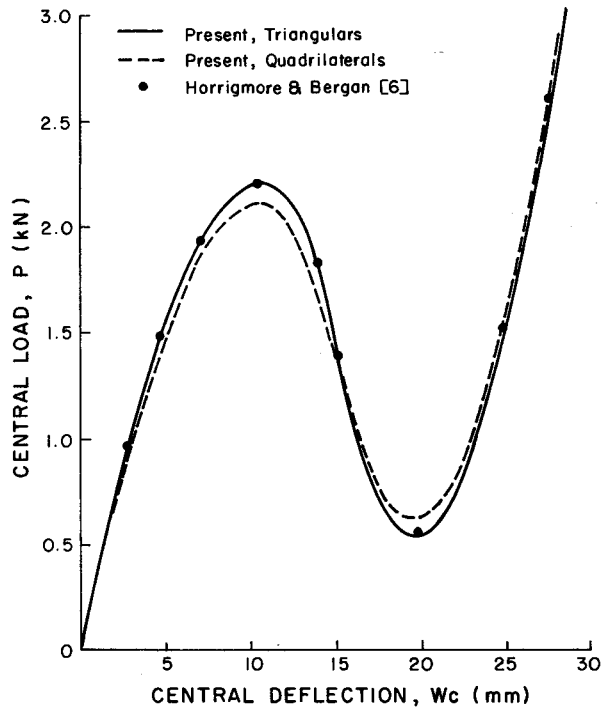

Fig. 6 Central deflection of hinged cylindrical shell.

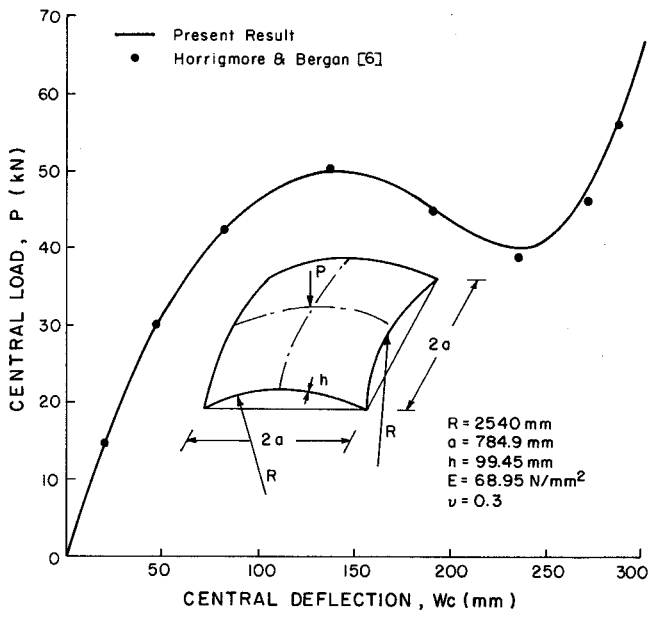

Fig. 7 Hinged spherical shell with a central load.

Example 5: Spherical Shell Subjected to Central Load

Figure 7 shows a spherical shell subjected to a concentrated load at the crown. All of the edges of the shell are hinged and immovable. A 5 × 5 mesh of triangular elements is used for one-quarter of the spherical shell. The resulting load-deflection curve at the crown, which is obtained by 16 increments, is depicted in Fig. 7 together with the result obtained by Horrigmore and Bergan[6] in which 29 increments are used. As indicated in Fig. 7, the present result agrees well with Horrigmore and Bergan's numerical solution, which was quoted close to the shallow shell series solution analysis obtained by Leicester.[21] This example is also studied by Bathe and Ho[22] using flat three-node triangular elements and an identical mesh with the one used here. Bathe and Ho[22] obtained similar results, but the maximum central displacement W_c = 298.35 mm was obtained using 19 load increments.[23]

Summary and Conclusions

The four-noded quadrilateral strain element developed by the authors is extended here to the nonlinear shell analysis. The von Karman assumptions and the updated Lagrangian formulation are used to derive the element tangent stiffness matrix. The transformation matrix of large rotations proposed by Argyris is adopted to account for the large rigid rotations. By using the quasiconforming element method, the element tangent stiffness matrix is given explicitly. In contrast to most finite elements obtained from numerical integration, the explicit form of the element stiffness matrix forms the most salient feature of the nonlinear element presented here. Since the element tangent stiffness matrices have to be evaluated numerous times in a nonlinear analysis, the explicit tangent stiffness matrix makes the results element much more computationally economical than those elements involving numerical integration in the nonlinear analysis of plates and shells.

The nonlinear postbuckling analysis of a number of structures is presented and compared with the existing analytical/numerical solutions of other works. The numerical examples show that the four-noded strain element presented here is not only simple and computationally efficient but also accurate. It renders that the nonlinear plate element with the explicit tangent stiffness matrices presented here is quite useful in the aerospace and nuclear industry where the nonlinear analysis of plates and shells is paramount.

Acknowledgments

The writers express appreciation for the support provided by the International Business Machines Corporation and Martin Marietta Manned Space Systems at New Orleans, Louisiana, through the project entitled Supercomputing in the Design and Manufacturing of Aerospace Structures.

References

[1]von Karman, T., and Tsien, H.-S., "The Buckling of Spherical Shells by External Pressure," *Journal of Aeronautical Sciences*, Vol. 7, 1939, pp. 43–50.

[2]Murray, D. W., and Wilson, E. L., "Finite-Element Post-Buckling Analysis of Thin Elastic Plates," *AIAA Journal*, Vol. 7, No. 10, 1969, pp. 1915–1920.

[3]Gallagher, R. H., and Thomas, G. R., "The Finite Element in Plate and Shell Instability Analysis," *Proceedings of the Fourth Australian Conference on Mechanics of Structures and Materials*, Brisbane, Australia, 1973, pp. 77–86.

[4]Sabir, A. B., and Lock, A. C., "The Application of Finite Elements to the Large Deflection Geometrically Non-Linear Behavior of Cylindrical Shells," *Variational Methods in Engineering*, edited by C. A. Brebbia and H. Tottenham, Southampton Univ. Press, Southampton, England, UK, 1973.

[5]Wood, R. D., and Zienkiewicz, O. C., "Geometrically Nonlinear Finite Element Analysis of Beams, Frames, Arches, and Axisymmetric Shells," *Computers & Structures*, Vol. 7, 1977, pp. 725–735.

[6]Horrigmore, G., and Bergan, P. G., "Nonlinear Analysis of Free-Form Shells by Flat Finite Elements," *Computer Methods in Applied Mechanics and Engineering*, Vol. 16, No. 1, 1978, pp. 11–35.

[7]Bathe, K. J., and Dvorkin, Z. N., "A Formulation of General Shell Elements—The Use of Mixed Interpolation of Tensional Components," *International Journal for Numerical Methods in Engineering*, Vol. 22, No. 3, 1986, pp. 697–722.

[8]Noor, A. K., Belytschko, T., and Simo, J. C. (eds.), *Analytical and Computational Models of Shells*, American Society of Mechanical Engineers, New York, 1989, p. 640.

[9]Shi, G., and Voyiadjis, G. Z., "Goemetrically Nonlinear Analysis of Plates by Assumed Strain Element with Explicit Tangent Stiffness Matrix," *Computers & Structures* (to be published).

[10]Tang, L., Chen, W., and Liu, Y., "Quasi-Conforming Element for Finite Element Analysis," *Journal of the Dalian Institute of Technology*, Vol. 19, No. 2, 1980, pp. 19–36 (in Chinese).

[11]Shi, G., and Voyiadjis, G. Z., "Efficient and Accurate Four-Node Quadrilateral C^o Plate Bending Elements Based on Assumed Strain Fields," *International Journal for Numerical Methods in Engineering*, Vol. 32, No. 5, 1991, pp. 1041–1055.

[12]Argyris, J., "An Excursion into Large Rotations," *Computer Methods in Applied Mechanics and Engineering*, Vol. 32, No. 1, 1982, pp. 85–155.

[13]Wempner, G. A., "Discrete Approximation Related to Nonlinear theories of Solids," *International Journal of Solids and Structures*, Vol. 7, No. 11, 1971, pp. 1581–1599.

[14]Riks, E., "The Application of Newton's Method to the Problem of Elastic Stability," *Journal of Applied Mechanics*, Vol. 39, 1972, pp. 1060–1066.

[15]Crisfield, M. A., "A Fast Incremental Interactive Solution Procedure that Handles Snap-Through," *Computers & Structures*, Vol. 13, 1981, pp. 52–62.

[16]Ramm, E., "Strategies for Tracing the Nonlinear Response Near Limit Points," *Nonlinear Finite Element Analysis in Structural Mechanics*, edited by W. Wunderlich, E. Stein, and K. G. Bathe, Springer-Verlag, New York, 1981, pp. 63–89.

[17]Kondoh, K., and Atluri, S. N., "A Simplified Finite Element Method for Large Deformation, Post-Buckling Analysis of Large Frames, Using Explicitly Derived Tangent Stiffness Matrics," *International Journal for Numerical Methods in Engineering*, Vol. 23, No. 1, 1986, pp. 69–90.

[18]Friedrichs, K. O., and Stoker, J. J., "Buckling of the Circular Plate Beyond the Critical Thrust," *Journal of Applied Mechanics*, 1942, pp. A7–14.

[19]Allman, D. J., "Improved Finite Element Method for the Large Displacement Bending and Post Buckling Analysis of Thin Plates," *International Journal of Solids and Structures*, Vol. 18, No. 9, 1982, pp. 737–762.

[20]Yang, T. Y., and Saigal, S., "A Curved Quadrilateral Element for Static Analysis of Shells with Geometric and Material Nonlinearities," *International Journal of Numerical Mech. Eng.*, Vol. 21, No. 4, 1985, pp. 617–635.

[21]Leicester, R. H., "Finite Deformations of Shallow Shells," *Journal of Engineering Mechanics*, Vol. 94, 1968, pp. 1409–1423.

[22]Bathe, K. J., and Ho, L. W., "A Simple and Effective Element for Analysis of General Shell Structures," *Computers & Structures*, Vol. 13, 1981, pp. 673–681.

[23]Hsiao, K.-M., "Nonlinear Analysis of General Shell Structures by Flat Triangular Shell Element," *Computers & Structures*, Vol. 25, 1987, pp. 665–675.